Azimuthal coil size and field quality in the main CERN Large Hadron Collider dipoles

P. Ferracin, W. Scandale, E. Todesco, and D. Tommasini
CERN, LHC Division, CH-1211 Geneva, Switzerland
(Received 7 August 2001; published 6 June 2002)

Field quality in superconducting magnets strongly depends on the geometry of the coil. Fiberglass spacers (shims) placed between the coil and the collars have been used to optimize magnetic and mechanical performances of superconducting magnets in large accelerators. A change in the shim thickness affects both the geometry of the coil and its state of compression (prestress) under operational conditions. In this paper we develop a coupled magnetomechanical model of the main Large Hadron Collider dipole. This model allows us to evaluate the prestress dependence on the shim thickness and the map of deformations of the coil and the collars. Results of the model are compared to experimental measurements carried out in a dedicated experiment, where a magnet model has been reassembled 5 times with different shims. A good agreement is found between simulations and experimental data both on the mechanical behavior and on the field quality. We show that this approach allows us to improve this agreement with respect to models previously used in the literature. We finally evaluate the range of tunability that will be provided by shims during the production of the Large Hadron Collider main dipoles.

DOI: 10.1103/PhysRevSTAB.5.062401 PACS numbers: 85.25.Ly, 85.70.Ay, 41.85.Lc, 62.20.Dc

I. INTRODUCTION

In superconducting magnets used for particle accelerators, the magnetic field strongly depends on the position of the conductors [1]. Therefore, a correct layout of the coil is crucial to obtain the field homogeneity needed for beam dynamics. In the case of the superconducting dipoles of the Large Hadron Collider (LHC) [2], under construction at the European Organization for Nuclear Research (CERN), the beam dynamics constraints require a control of field homogeneity up to 10^{-5} for some components [3]. This implies that the standard deviation of the cable positioning is around 0.03 mm [4], leading to global tolerances of the coil layout of less than 0.1 mm. Such tolerances must be kept under the assembly forces that compress the coil with an azimuthal prestress of several tens of MPa.

To achieve these challenging goals during a production phase that will last a few years, some flexibility has been allowed in the magnet design: epoxy fiberglass spacers (shims) are placed between the coil and the austenitic steel collars in the pole region. Shim thickness can therefore be varied to optimize the magnet performances. Adjustable shims have been used in magnets for the Tevatron [5], for the High Electron Ring Accelerator (HERA) [6], in the Superconducting Super Collider (SSC) magnet prototypes [7], and for the Relativistic Heavy Ion Collider (RHIC) [8,9]. They aim at optimizing either the mechanical or the magnetic performance. In the first case, adjustable shims compensate variations of the azimuthal size of the coil to obtain an optimal azimuthal prestress. This strategy has been followed both in the LHC and in the SSC dipole prototype phases [2,7] and as a first guess for the shim dimension in the HERA dipoles [6]. In the second case, an adjustable shim is used to modify the coil size under compression to reach an optimal magnetic field. If we assume a constant collar cavity and a constant coil size, the adjustable shim will also modify prestress. In a production phase one has a mix of both cases, where an acceptable range has been defined for the prestress, and shims are used both to stay in this range and to reach the optimal coil size for field quality (see for instance the experience of Tevatron [5], HERA [6], and RHIC [8,9]).

In previous works [1,5,10], the magnetic effect of a shim thickness increase δ has been modeled by a uniform azimuthal compression δ of the coil: this first-order approximation is based on the assumption that the rigidity of the collar cavity is much larger than the rigidity of the coil. Nevertheless, since the cavity rigidity is not infinite, a shim thickness increase leads to a different cavity deformation, bringing additional contributions to the field harmonics. A first step towards a coupled magnetomechanical model of the dipole has been made for the LHC short model dipoles: in Ref. [11] a δ increase of the shim is modeled as a coil compression of $\alpha\delta$, where $\alpha < 1$ is related to the measured collar deflection. Also in this case, variations in the radial geometry of the coil are neglected. Unfortunately, field quality is extremely sensitive on conductor positions, and therefore these effects cannot be neglected if one aims at a precise estimate of the dependence of field quality on shim size.

In this paper we propose a finite element model of the dipole cross section based on the properties of its components (see Ref. [12] for the coil thermomechanical properties). A novel approach has been defined to model the collaring procedure in the finite element code through equivalent properties of the coil. This mechanical model allows us to compute coil and collar deformations and the effect of pole shim thickness on coil azimuthal prestress. Results are then used by a magnetostatic code [13] to evaluate the impact on field quality. All the quantities

derived by this complex magnetomechanical model have been validated through a dedicated experiment, where a 1 m long superconducting dipole magnet model has been reassembled 5 times with different shim sizes. At the end of each assembly procedure, prestress, collar deflection, and magnetic field have been measured and compared to the model. Results show that a precise evaluation of the dependence of field quality on shim thickness cannot neglect the mechanical features of the problem, i.e., radial deformations of the coil and the deflection of the collars.

In Sec. II we describe the coil layout and the pole shims. The finite element model used to work out the magnetomechanical behavior of the magnet is briefly described in Sec. III. The experimental setup used to measure the sensitivity of the magnetic field on the shim sizes is described in Sec. IV. Experimental and numerical results are compared in Sec. V. Appendix A describes the collaring procedure. The method to define coil mechanical properties implemented in the model is given in Appendix B.

II. COIL LAYOUT

The main LHC dipole is about 15 m long and it is made up of superconducting coils clamped by austenitic steel collars (see Fig. 1). The collars are surrounded by an iron yoke contained by a stainless steel shrinking cylinder. An azimuthal compression (prestress) of the coils between 60 and 90 MPa at 300 K [14] is required at the end of the collaring procedure to keep them under compression in all the conditions up to the nominal field of 8.3 T. In this magnet design, the yoke has only a minor effect on coil prestress.

The cross section of the LHC dipole coil (see Fig. 2) features two layers of superconducting cables of the Rutherford type. A quadrant of the coil is composed of six conductor blocks, spaced by three copper wedges. Inner and outer pole shims are placed between the collars and inner and outer layers, respectively (see Fig. 3). A variation of the shim dimension directly affects the azimuthal coil size and induces a prestress change. Any variation of the shims aimed at correcting field quality must take into account consequences on prestress and ensure that the azimuthal coil compression stays in the allowed range.

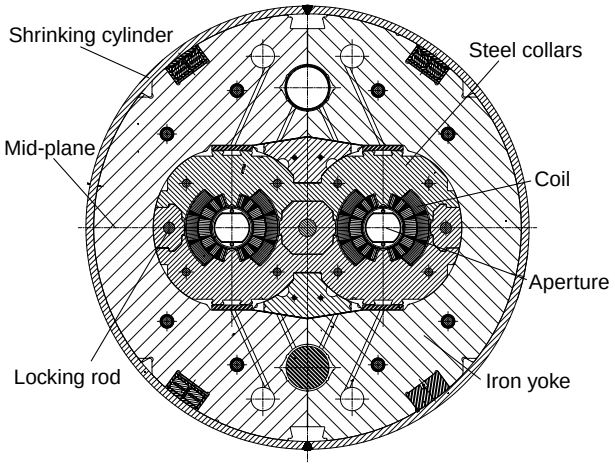

FIG. 1. LHC dipole cross section.

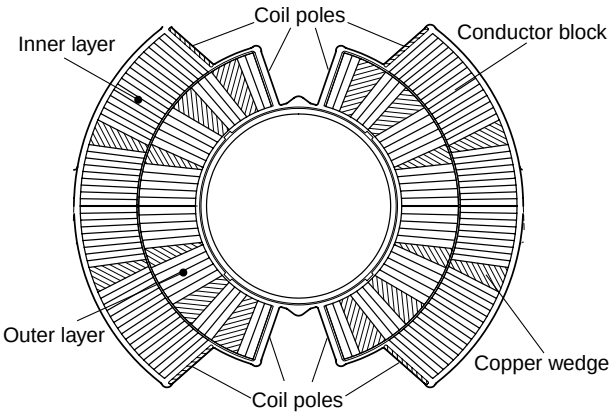

FIG. 2. Cross section of the LHC dipole coil.

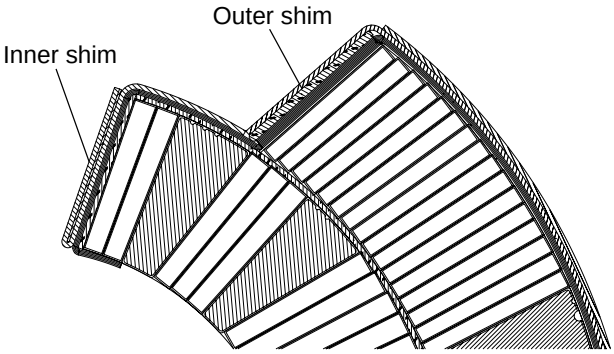

FIG. 3. Pole shims of the LHC dipole coil.

III. FINITE ELEMENT MODEL

A structural two-dimensional model of the dipole cross section has been developed at CERN [15–17] using the finite element code ANSYS [18]. Different material properties are associated with the corresponding areas of the cross section, and interfaces between materials are modeled through contact elements. Conductor blocks (made of cable and insulation) are modeled as an homogeneous material.

During the collaring procedure, the coils are compressed to a maximum peak prestress up to the insertion of the locking rods; then, the exerted pressure is released and only a fraction of the peak prestress is left.

Since the coils are affected by well-known hysteresis phenomena [12,19,20], their final mechanical state after

collaring will depend not only on the final prestress but also on the stress-strain path followed during the collaring. Therefore, one should build two finite element models, one for the loading phase up to the insertion of the locking rods and one for the prestress release phase. The two models should have different coil mechanical properties, namely, the loading and the unloading ones, respectively, and the solution of the loading model should be used as the initial condition of the unloading phase. In this paper we propose an alternative approach, based on experimental measurements of the stresses during the collaring procedure (see Appendix A). We use a single-step model where loads are given through contact element interferences. Therefore we have to define an "equivalent" elastic modulus of the coils that takes into account the collaring procedure. On the one hand, this approach allows us to considerably simplify the model without losing the crucial features of the problem. On the other hand, the model is more accurate since it is based on the measured prestresses during collaring. The approach to work out the equivalent elastic modulus is described in Appendix B. In Sec. V we will show that this is crucial to obtain correct estimates of the dependence of the coil prestress on the shim size.

Once the material properties are defined, interferences between coil pole and collars are set to correctly reproduce the nominal azimuthal prestress in the magnet. Then, variations of these interferences of 0.1 mm are applied on the inner and on the outer layers, keeping the fourfold symmetry of the coil. The corresponding variations of azimuthal prestress, vertical diameter of the collars, and coil deformations are computed. Coil displacements are then transferred to a magnetostatic code [13] to evaluate the impact on the magnetic field.

IV. EXPERIMENTAL SETUP

A 1 m long dipole magnet has been reassembled 5 times with different shims. The shim thickness has been changed by ± 0.15 mm, for both layers. This variation has been done in the two apertures at the same time, keeping the left-right and top-bottom symmetries. First, the configuration with nominal shims has been assembled and measured. Then, the inner shims have been changed keeping constant the outer ones; finally, the same has been done for the outer layer, keeping the nominal inner shim. For each of the five cases, the magnet has been assembled without the iron yoke and the shrinking cylinder; just the so-called collared coil at ambient temperature has been studied.

The prestress during the collaring (see Appendix A) and the final prestress have been measured for the two apertures by means of capacitive gauges [21] set at coil poles. The sensitivity of these gauges is 1 MPa. At the end of the collaring, the vertical diameter of the collar has been measured and magnetic measurements have been carried out.

V. RESULTS

Here, we compare the results of the finite element model with the experimental data that are presented with a statistical error of $2 \times$ rms, giving a 95% confidence level in the hypothesis of a Gaussian distribution.

The field shape of the dipole is described using the standard multipolar expansion of the magnetic field

$$B_y + iB_x = B_1 \sum_n (b_n + ia_n) \frac{(x + iy)^{n-1}}{R_{\text{ref}}^{n-1}}. \quad (1)$$

In this expansion, b_n and a_n are the multipolar coefficients. They are expressed in 10^{-4} units with respect to the main field. The odd normal terms b_3, b_5, … are the so-called allowed multipoles and are due to contributions that respect the fourfold symmetry of the dipole cross section. Even normal multipoles b_2, b_4, … and skew components a_2, a_3, a_4, … are due to left-right and top-bottom asymmetries, respectively. Since in our case the geometry of the coil layers is varied keeping these symmetries, only the odd normal multipoles are influenced. The reference radius R_{ref} is set to 17 mm, i.e., about $2/3$ of the magnet aperture, which is the conventional value for the arc magnets of the LHC.

A. Correlation between pole shim thickness and coil prestress

In Table I we give the shim thickness variations and the measured azimuthal prestress of the collared coil in the two apertures. A variation of the shim dimension mainly affects the prestress of the corresponding layer: in fact, a prestress variation of about 20 MPa in one layer provokes a modification of the prestress in the other layer within 3 MPa. The same weak mechanical coupling of the two layers is found in the finite element model.

Prestress versus shim thickness of the same layer features a linear behavior, with similar slopes in the two apertures (see Fig. 4). Best fits with straight lines show that an additional shim of 0.1 mm increases the prestress by 12 to 13 MPa. Our finite element model provides the same result for the inner layer, while it underestimates the prestress variation on the outer layer by about 3 MPa (see Table II).

TABLE I. Shim thickness variation (mm) and corresponding prestress (MPa) for the inner and the outer layers, experimental data.

Δ shim (mm)		Prestress Ap. 1 (MPa)		Prestress Ap. 2 (MPa)	
Inner	Outer	Inner	Outer	Inner	Outer
0.00	0.00	49	51	44	60
0.15	0.00	67	49	62	60
−0.15	0.00	30	51	28	60
0.00	0.15	50	72	46	79
0.00	−0.15	52	32	49	39

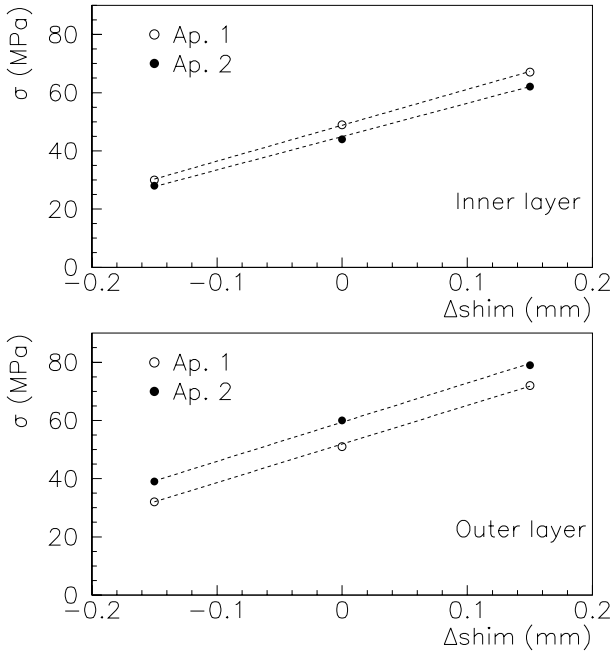

FIG. 4. Prestress σ (MPa) versus shim thickness variation (mm) for the inner and outer layers and for the two apertures (Ap. 1 and Ap. 2), experimental data, and linear fit.

TABLE II. Effect of a 0.1 mm thicker shim on the azimuthal prestress (MPa).

	Inner layer	Outer layer
Measurements	12 ± 1	13 ± 1
Finite element model	12	10

This may be due to a slightly different mechanical behavior between straight conductor stacks, which have been measured to work out the equivalent elastic modulus (see Appendix B), and conductor arcs. Most likely, the outer layer is more sensitive to this difference, since it features blocks with a higher number of conductors. Nevertheless, we point out that using the unloading elastic modulus of the coil one would have obtained a severe overestimate of the prestress dependence on the shim size (about a factor of 2).

B. Correlation between coil prestress and collar deformation

The mechanical behavior of the cavity where the coil is placed [22] can be studied by measuring the variation of the vertical diameter of the collars due to a prestress increase in the coil.

This is linked to the rigidity of the collars, which is a combined effect of the collar material (stainless steel) and of its rather complex geometry. The vertical diameter of the collars has been measured in the five collared coils. The comparison with the results from the finite element model is very good (see Table III).

TABLE III. Effect of an increase of 10 MPa of the average prestress on the collar vertical dimension.

	Δ diameter (mm)
Measurements	0.036 ± 0.006
Finite element model	0.037

C. Analysis of coil deformations

The finite element model can provide the whole map of deformations, which are not purely azimuthal, induced by the variation of the shim thickness. In Figs. 5 and 6 we plot the nominal geometry of the coils (solid lines) and the displacements induced by a shim variation of 0.1 mm on the inner and on the outer layer, respectively (dashed lines). Displacements are magnified by a factor of 50 to make the figure easier to analyze and to interpret.

The first graph shows that the variation on the inner layer shim provokes an inner coil azimuthal compression, but also a radial deformation. The azimuthal displacement of the inner coil is around 0.095 mm, i.e., 5% less than the additional shim thickness. The inner coil is also radially shifted in the outward direction up to 0.017 mm; the maximum amplitude of this radial movement is reached in correspondence to the pole of the outer layer (around 55°). A reduction of this amplitude is then observed on the last conductors of the inner layer (at around 75°), close to the pole. Therefore, this shows that coil deformations cannot be described by a simple elliptic mode. This importance of high-order modes in radial displacements has been already observed in the analysis of coil deformations for the main LHC dipoles [23].

The outer coil has a very small increase of the azimuthal size (0.003 mm) due to the weak cross talk between the two layers. It also features a radial displacement of around 0.010 mm. A similar situation holds for the left part of the coil (i.e., towards the center of the magnet), the only difference being a smaller radial displacement in the coil midplane, due to the two-in-one collar geometry. A 0.1 mm thicker outer shim provokes an azimuthal displacement of the outer coil pole of around 0.090 mm (see

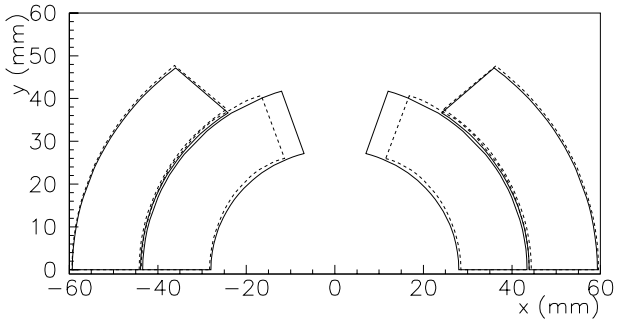

FIG. 5. Nominal coil geometry (solid line) and deformed geometry (dashed line) induced by a 0.1 mm thicker shim in the inner coil. Deformations are magnified by a factor of 50.

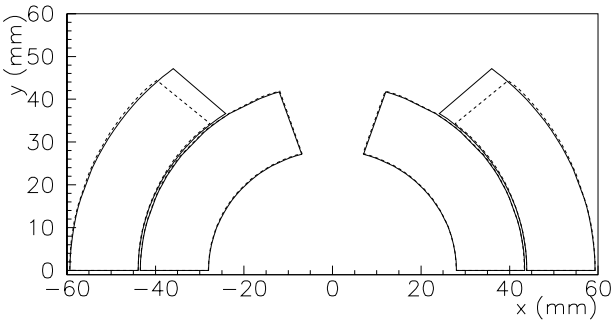

FIG. 6. Nominal coil geometry (solid line) and deformed geometry (dashed line) induced by a 0.1 mm thicker shim in the outer coil. Deformations are magnified by a factor of 50.

Fig. 6). Radial displacements of the outer coil are around 0.005 mm on the pole, while practically no displacements are observed in the inner coil (less than 0.003 mm).

This analysis shows that our finite element model foresees a coil displacement more complex than the one predicted by the simple model based on pure azimuthal compression with an infinitely rigid collar. In the next section we will evaluate the impact of these displacements on field harmonics, cross-checking the calculations with the magnetic measurements.

D. Correlation between pole shim thickness and allowed field harmonics

Room temperature magnetic measurements of the b_3 and the b_5 in the collared coil versus the shim thickness are shown in Figs. 7 and 8. Also in this case, one finds a good linearity and a similar slope for both apertures. Best fits with a straight line provide the dependence of harmonics on shim thickness, which are given in Table IV. Only the case of the allowed coefficients b_3, b_5, and b_7 has been analyzed, with the higher orders being weakly dependent on the shim size.

In the same table, we list the results of simulation based on three different approaches. We first consider a purely azimuthal compression of the coil by 0.1 mm, assuming that the copper wedges are infinitely rigid (row "uniform compression"). This approximation systematically overestimates the measured sensitivities of 20% (b_3 and b_7) to 60% (b_5). Taking into account the experimental errors, the discrepancy is significant for b_3 and b_5.

Then, following the approach of Ref. [11], we include the measured collar deflection. A 0.1 mm wider shim increases azimuthal prestress of around 12 MPa on one layer (see Table II). This increases the average prestress of 6 MPa and corresponds to a 0.011 mm increase in the vertical radius (see Table III). The collar deflection compensates the additional shim thickness that will drop from 0.1 to 0.089 mm. Therefore, our sensitivity estimates must be reduced by 11% (see Table IV, row "compensated compression." In this way we recover the agreement within experimental errors for b_3, but not for b_5.

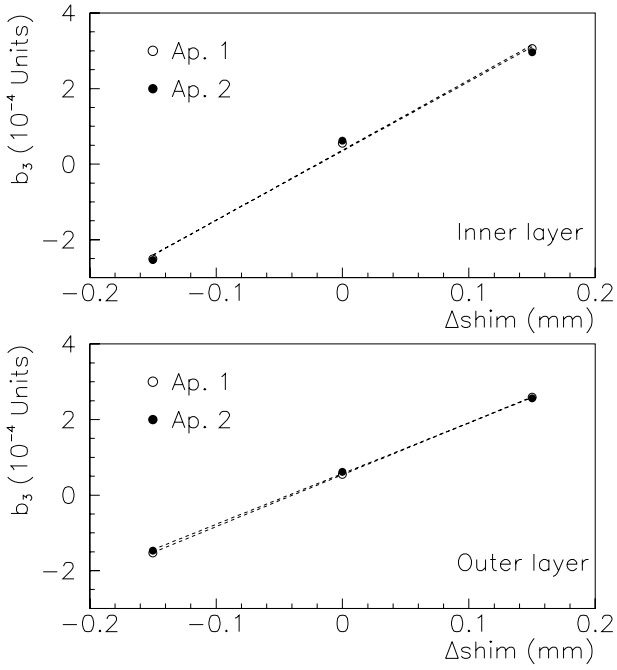

FIG. 7. b_3 (10^{-4} units) versus shim thickness variation (mm) for the inner and outer layers and for the two apertures (Ap. 1 and Ap. 2), experimental data, and linear fit.

Results of the finite element model recover an agreement also for b_5. This is mainly due to radial deformations that were neglected in the previous approaches. One concludes that our capability of modeling the mechanical behavior of the coil is sufficiently precise not only in terms of stresses, as has been shown in the previous section, but also in terms

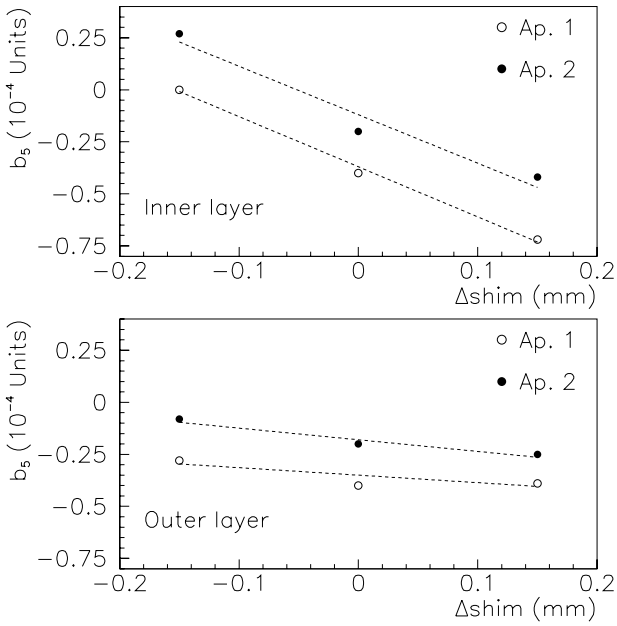

FIG. 8. b_5 (10^{-4} units) versus shim thickness variation (mm) for the inner and outer layers and for the two apertures (Ap. 1 and Ap. 2), experimental data, and linear fit.

TABLE IV. Effect on an additional shim of 0.1 mm on allowed multiples (10^{-4} units, $R_{\text{ref}} = 17$ mm): experimental data and comparison with the finite element model and with the uniform azimuthal compression approximations.

Δb_3	Inner layer	Outer layer
Uniform compression	+2.18	+1.62
Compensated compression	+1.96	+1.46
Finite element model	+1.88	+1.46
Measurements	+1.85 ± 0.26	+1.36 ± 0.10
Δb_5	Inner layer	Outer layer
Uniform compression	−0.40	−0.08
Compensated compression	−0.36	−0.07
Finite element model	−0.29	−0.05
Measurements	−0.24 ± 0.06	−0.05 ± 0.04
Δb_7	Inner layer	Outer layer
Uniform compression	+0.15	−0.02
Compensated compression	+0.14	−0.02
Finite element model	+0.12	−0.02
Measurements	+0.13 ± 0.04	−0.01 ± 0.00

of displacements, since it allows a reliable estimate of the impact of deformations on the magnetic field.

The above analysis concerns the collared coil that is the first stage at which magnetic measurements are taken. By these measurements assembly errors or drifts of the dimensions of the magnet components can be detected and corrected during series production. The whole magnet (collared coils within the iron yoke and the shrinking cylinder) features different sensitivities of the field on the shim size. This is due to the magnetic influence of the iron yoke.

In Table V we estimate this effect using our magnetomechanical model. The values for the whole magnet are compared with the ones computed for the collared coil, already shown in Table IV. One observes that the cold mass has a lower sensitivity by around 20%: this is due to a scale down of the multipoles since the main field is enhanced by the iron yoke of about 20%.

Since the maximum admissible variation of shim thickness is ±0.12 mm, due to the ±15 MPa limitation in the azimuthal prestress (see Ref. [14] and Table II), one obtains the order of magnitude of tunability provided by shim thickness: for the b_3 one can obtain up to ±4.0 units, while one has ±0.35 and ±0.15 units for the b_5 and the b_7, respectively. Indeed, since only two parameters are available for optimization (inner and outer shim thicknesses), some values in this range cannot be obtained: for instance, the maximum positive variation of b_3 is reached for a shim increase on both layers and therefore cannot correspond to a positive variation of b_5.

TABLE V. Effect on an additional shim of 0.1 mm on allowed multiples (10^{-4} units, $R_{\text{ref}} = 17$ mm): finite element results for collared coil and assembled cold mass at room temperature.

Δb_3	Inner layer	Outer layer
Collared coil	+1.88	+1.46
Cold mass	+1.57	+1.22
Δb_5	Inner layer	Outer layer
Collared coil	−0.29	−0.05
Cold mass	−0.24	−0.04
Δb_7	Inner layer	Outer layer
Collared coil	+0.12	−0.02
Cold mass	+0.10	−0.02

VI. CONCLUSIONS

In this paper we analyzed how the field quality of the main LHC dipole can be tuned by changing the coil geometry with fiberglass spacers (shims) placed on the coil pole faces. In a first approximation, a δ mm thicker shim leads to a decrease in the azimuthal coil size of the same amount, since the collars are more rigid than the coil. Nevertheless, a different shim size also induces a variation in the azimuthal prestress and changes the patterns of coil deformations, thus affecting field quality.

We propose a coupled magnetomechanical model to precisely evaluate the dependence of field quality on shim thickness. The mechanical model is implemented in a finite element code based on the measured mechanical properties of the dipole component. A crucial feature of our finite element model is the coil elasticity that takes into account the stress-strain path followed during the collaring procedure. This novel approach allows us to describe the dipole mechanics through a simple one-step model, based on experimental measurements of prestress during collaring. This model provides the dependence of the prestress on shim size that is an important parameter that sets the maximum admissible variation of the shim thickness. Estimated coil deformations are then transferred to a magnetostatic code to evaluate the impact on field quality.

A dedicated experiment on a 1 m long dipole model has been carried out to validate both the mechanical and the magnetic effects of a change in shim dimension. The model has shown a good agreement with experimental data on stresses and deformations, such as the measurements of the vertical dimension of the collars and of the sensitivity of prestress on shim size. The dependence of the odd low-order multipoles on the shim size is also in good agreement with experimental results. On the other hand, simplified models previously used in the literature show significant discrepancies with the experimental results. In particular, higher-order radial modes of deformations are shown to have a strong influence on the b_5. One finally obtains the range of tunability of low-order odd multipoles provided by pole shims for the main LHC dipoles.

ACKNOWLEDGMENTS

We would like to acknowledge O. Pagano for the magnetic measurements and H. Kummer, M. Parent, and

F. Rougemont for the prestress measurements. We wish to thank G. Spigo for endless discussions about coil prestress during collaring. A special thanks to L. Rossi for carefully reading the manuscript and for useful comments.

APPENDIX A: PRESTRESS MEASUREMENTS DURING COLLARING

As already mentioned in the introduction, the coil is clamped by means of austenitic steel collars. The collaring can be defined as the procedure to position the coils into the collar cavities, under a given azimuthal prestress. Collars and coils are compressed in a press in order to insert the collaring rods, which lock the collars. After rod insertion, the press is released: coil prestress decreases because of the collar elastic deformation and because of the clearance between the rods and the collar holes.

We define as *relaxation* [24] the ratio k between the remaining coil azimuthal stress after the collaring σ^c and the maximum coil azimuthal stress (peak stress) reached during the collaring phase σ^p; that is

$$k = \frac{\sigma^c}{\sigma^p}. \tag{A1}$$

This ratio provides the stress path followed by the coil during the magnet assembly. In Fig. 9 the values of the peak and of the remaining stress on the coil in the five different collarings are plotted. Some dependence of the relaxation on the peak stress is observed. A linear fit of relaxation versus peak prestress gives

$$k_{\text{in}} = 0.002\sigma^p_{\text{in}} + 0.54, \tag{A2}$$

and

$$k_{\text{ou}} = 0.002\sigma^p_{\text{ou}} + 0.48, \tag{A3}$$

where k_{in} and k_{ou} are the relaxations for the inner and the outer layers, and σ^p_{in} and σ^p_{ou} are the peak stresses in MPa reached during the collaring on the inner and the outer layers. The linear dependence of k on σ^p gives rise to the parabolic dependence of σ^c on σ^p observed in Fig. 9.

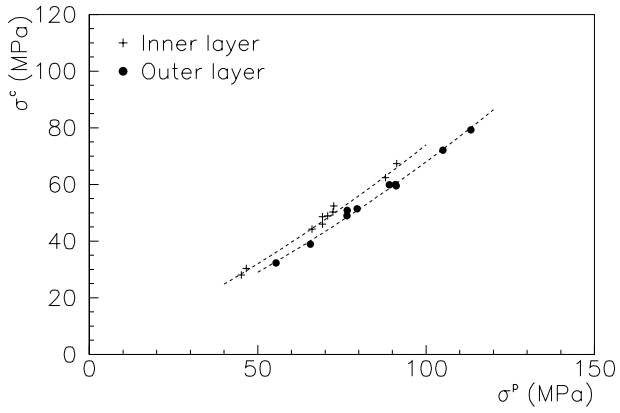

FIG. 9. Residual azimuthal stress on the coil σ^c (MPa) versus peak σ^p stress (MPa) during five collarings of the 1 m long prototype.

APPENDIX B: MECHANICAL PROPERTIES OF THE COIL

The superconducting coil of the LHC is made up of copper wedges and conductor blocks. The latter are modeled in the finite element model as zones with global mechanical properties, which include cables and insulation layers. The coil behavior under compression is the crucial parameter to obtain a correct evaluation of prestress and deformations. As has been described in [12], the stress-displacement curve of a stack of coil conductors is characterized by an hysteresis whose width depends on the peak stresses reached during the compression cycle (see Fig. 10). This mechanical hysteresis is relevant to our problem, since during the assembly procedure the coil is first loaded up to a peak prestress and then unloaded (see Appendix A). A finite element model should be implemented in two steps: a coil compression up to the peak prestress, based on coil mechanical properties during the loading phase. Stresses and deformations obtained by this model should then be used as an initial condition in a second model, where coil mechanical properties during unloading should be used.

We propose an alternative approach based on a single-step model. The collaring procedure is not explicitly modeled, and loads are given through contact elements placed between the coil and the collars. The prestress in the coil after collaring is obtained by choosing the appropriate interferences associated with the contact elements. Variations of the shim dimensions are then simulated by a change of these interferences.

To choose the elastic modulus of the coil to be implemented in the model, we have to take into account the collaring procedure. A coil collared with different shims

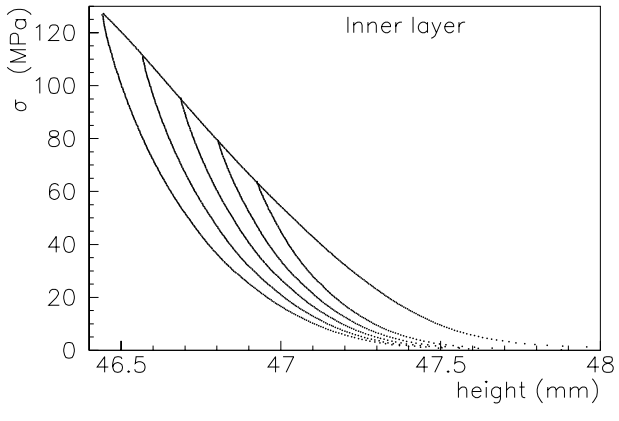

FIG. 10. Stress σ (MPa) at ambient temperature versus total height of a stack of 22 conductors for the inner layer, loading and unloading curves from different peak stresses (treated experimental data).

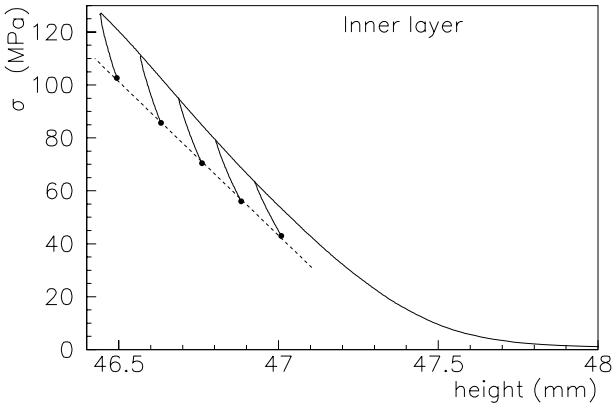

FIG. 11. Equivalent stress-displacement curve (dashed line) for the coil inner layer.

will reach different peak prestresses and then relax to a prestress value given by Eq. (A1). In Fig. 11 we show the path followed by the coil in the stress-displacement plane for five collarings (solid lines). The five markers are the points reached by the coil after the collaring. They can be fitted by a straight line (dashed line in Fig. 11) whose slope is proportional to an equivalent elastic modulus which is smaller than both the unloading and the loading elastic moduli. The implementation of these equivalent properties allows us to reach the correct stress-displacement status of the coil in a single-step model.

In our case, stress-displacement curves of both the inner and the outer layers of the LHC cable measured in Ref. [12] have been postprocessed using the measured relaxation given by Eqs. (2) and (3). The equivalent elastic moduli E^{eq}

$$E_{\mathrm{in}}^{\mathrm{eq}} = 5.5\ \mathrm{GPa}, \qquad E_{\mathrm{ou}}^{\mathrm{eq}} = 5.1\ \mathrm{GPa} \qquad \text{(B1)}$$

are obtained for the inner and the outer layers, respectively. Through this postprocessing of the stress-displacement curve of a conductor stack, the stress history of the coil during the collaring is taken into account and, as presented in Sec. V, a good agreement between the numerical results and the experimental data of the prestress sensitivity is obtained.

[1] K.-H. Mess, P. Schumser, and S. Wolf, *Superconducting Accelerator Magnets* (World Scientific, Singapore, 1996), Chap. 5, Sect. 1, p. 66.

[2] M. Modena *et al.*, in *Proceeding of the 2001 Particle Accelerator Conference, Chicago, IL,* edited by P. Lucas and S. Webber (IEEE, Piscataway, NJ, 2001), p. 186; CERN LHC Project Report No. 487, 2001.

[3] S. Fartoukh and O. Bruning, CERN LHC Project Report No. 501, 2001.

[4] P. Ferracin, W. Scandale, E. Todesco, and R. Wolf, Phys. Rev. ST Accel. Beams **3**, 122403 (2000); CERN LHC Project Report No. 460, 2000.

[5] A. V. Tollestrup, Fermilab Report No. UPC-86, 1979.

[6] A. Bonito Oliva, P. Gagliardi, R. Penco, and P. Valente, Cryogenics **30**, 589 (1990).

[7] A. Devred *et al.*, in *Physics of Particle Accelerators*, edited by M. Month and M. Dienes, AIP Conf. Proc. No. 249 (AIP, New York, 1992), p. 1309.

[8] M. D. Anerella, D. H. Fisher, E. Sheedy, and T. McGuire, IEEE Trans. Magn. **32**, 2059 (1996).

[9] R. C. Gupta *et al.*, in *Proceedings of the Fifteenth International Conference on Magnet Technology, Beijing, 1997*, edited by L. Liangzhen, S. Guoliao, and Y. Luguang (Science Press, Beijing, 1997), p. 110.

[10] T. Ogitsu and A. Devred, Rev. Sci. Instrum. **65**, 1998 (1994).

[11] Z. Ang, L. Bottura, S. Russenschuck, A. Siemko, D. Tommasini, and L. Walckiers, IEEE Trans. Appl. Supercond. **10**, 53 (1999); CERN LHC Project Report No. 359, 1999.

[12] K. Couturier, P. Ferracin, E. Todesco, D. Tommasini, and W. Scandale, IEEE Trans. Appl. Supercond. (to be published).

[13] S. Russenschuck, in *Proceedings of the First International ROXIE Users Meeting and Workshop, Geneva, 1998*, edited by S. Russenschuck (CERN, Geneva, 1998), p. 1.

[14] CERN Report No. IT-2997/LHC/LHC, 2001.

[15] M. Bona, M. Modena, and D. Perini, in *Proceedings of the ANSYS Fifth International Conference and Exhibition, Pittsburgh, 1991*, edited by D. E. Dietrich (IEEE, New York, 1991), p. 17.30.

[16] M. Bona and D. Perini, IEEE Trans. Magn. **28**, 358 (1992).

[17] M. Bajko, P. Fessia, and D. Perini, IEEE Trans. Appl. Supercond. **10**, 81 (2000).

[18] ANSYS, licensed by and trademark of Swanson Analysis Inc., Houston, PA.

[19] R. B. Meuser, S. Caspi, and W. S. Gilbert, IEEE Trans. Magn. **17**, 2320 (1981).

[20] M. Reytier, A. Devred, M. Durante, C. Gourdin, and P. Vedrine, IEEE Trans. Appl. Supercond. **11**, 3066 (2001).

[21] N. Siegel, D. Tommasini, and Y. Vanenkov, in *Proceedings of the Fifteenth International Conference on Magnet Technology, Beijing, 1997* (Ref. [9]), p. 110; CERN LHC Project Report No. 173, 1998.

[22] J. Strait, J. Kerby, R. Bossert, J. Carson, G. Spigo, and J. R. Turner, in *Proceedings of the 1991 Particle Accelerator Conference: Accelerator Science and Technology, San Francisco, 1991*, edited by L. Lizama and J. Chew (IEEE, New York, 1991), p. 2176.

[23] P. Ferracin, W. Scandale, E. Todesco, and P. Tropea, in *Proceeding of the 1999 Particle Accelerator Conference, New York, 1999*, edited by A. Luccio and W. MacKay (IEEE, Piscataway, NJ, 1999), p. 3206; CERN LHC Project Report No. 287, 1999.

[24] G. Spigo (private communication).